EFFECT OF DESERT PARTICULATE COMPOSITION ON HELICOPTER ENGINE DEGRADATION RATE

Nicholas Bojdo* & Antonio Filippone
The University of Manchester
Manchester M13 9PL
United Kingdom

ABSTRACT

Abrasive, short-term damage to helicopter engines by quartz particles can be mitigated by the use of an inlet particle separator. However, such devices fail to remove the finest particles that have significantly different mineralogy to quartz. If these particles reach the hot end components, they may form deposits on the vane surfaces, or clog cooling holes. In the former case, a choking effect is created leading to a reduction in the surge margin; in the latter, an increase in heat transfer to the blade thence reduction in life may result. Prediction of this is limited by the myriad of contributory factors: the likelihood of a particle adhering to a surface depends on its phase and viscosity which changes along its path; the rate of change of state depends on the physical and chemical properties of the particle, which vary according to global location and inlet separator effectiveness. This contribution summarises the process of turbine degradation in desert-based helicopters, and proposes a novel approach to its prediction.

1 INTRODUCTION

Modern day rotorcraft are often required to operate to and from unprepared landing sites. In desert environments this can lead to the disturbance of loose sediment from the ground, creating a cloud of dust that soon envelopes the whole aircraft in a situation known as brownout (see Fig. 1). In such an event, particulate is drawn into the engine inlets. Almost all rotorcraft operating in such environments are fitted with engine air particle separators, or EAPS, which remove the majority of the particulate with varying degrees of success, depending on the type of device employed[1].

Fig. 1: RAF Merlin Helicopter Creates a 'Brownout' Dust Cloud Landing in Afghanistan. (Images: © Sgt. Steve Blake, UK Ministry of Defence.[2]).

A recent study by Barone et al.[3] demonstrated that an inertial particle separator (based on patent Ref.[4]) could achieve an efficiency of 92% removal of AC Coarse test dust (diameter range 0-200μm; mean diameter 36.8μm), although similar studies on IPS in the literature report lower efficiencies[5]–[7]. However, samples taken from typical locations of operation have shown AC Coarse test dust to be an inaccurate representation of the typical size distribution likely to be ingested by helicopter engines in desert environments. Furthermore, of the finer particles that avoid capture, samples taken from typical regions of operation are found to have mineral compositions much different to that found in test dust[8].

The importance of mineral composition should not be underestimated. While diameter, shape and density all influence the trajectory through the fluid, the mineralogy of the particle – that is, the way in which the constituent elements combine to make a mineral – is the key to predicting the likelihood of adhesion to a surface in the hot section of a gas turbine engine. Furthermore, when several minerals are combined in molten form, their product may exhibit radically different chemical properties to the original influent particulate that could lead to corrosion of component surfaces.

The damage to component surfaces is wide-ranging and affects each stage of the gas turbine. A comprehensive review of the research into erosion and deposition in turbomachinery is presented by Hamed & Tabakoff[9]. During the first Gulf War, the severity of damage to unprotected Chinook engines led to rejection rates of 20 to 40 engines per 1000 flight hours. Compressor blades bear the brunt of the damage from hard quartz particles, suffering blunted leading and trailing edges, and pitted pressure surfaces, while turbine blades experience considerable build-up of molten deposits as impurities solidify on film cooled surfaces. Such damage is pictured in Fig. 2. Combustor walls may also become glazed, reducing the flow path area.

Cooled turbine blades suffer a secondary

* Honorary Lecturer & Research Associate. School of MACE, Pariser Building. Corresponding Author. Email: Nicholas.Bojdo@manchester.ac.uk

problem too, in that cooling holes can become blocked by particulate entering compressor bleed line, heating as they pass through internal cooling ducts, and sticking to hole surfaces through inertia as the cooling air navigates the labyrinth-like passages. Smialek et al.[8] report that inspection of Gulf War engines revealed crusty deposits on leading edges of vane platforms and a talc-like powdery substance in the cooling passages of turbine discs. The process is non-linear and exponential by nature: as particulate builds up, it acts as an insulating layer thus reducing the heat transfer from coolant to blade. The subsequent elevated blade temperature leads to acceleration of further sticking and thickening of the insulating layer [10]. Clogging of cooling holes in turbine blades and vanes can have a short term positive effect on engine performance as compressor bleed is reduced. This reduces the surge margin but increases the overall engine efficiency. However, the overheating of the nozzles and blades significantly reduces their lifetime from thousands to hundreds of hours[11].

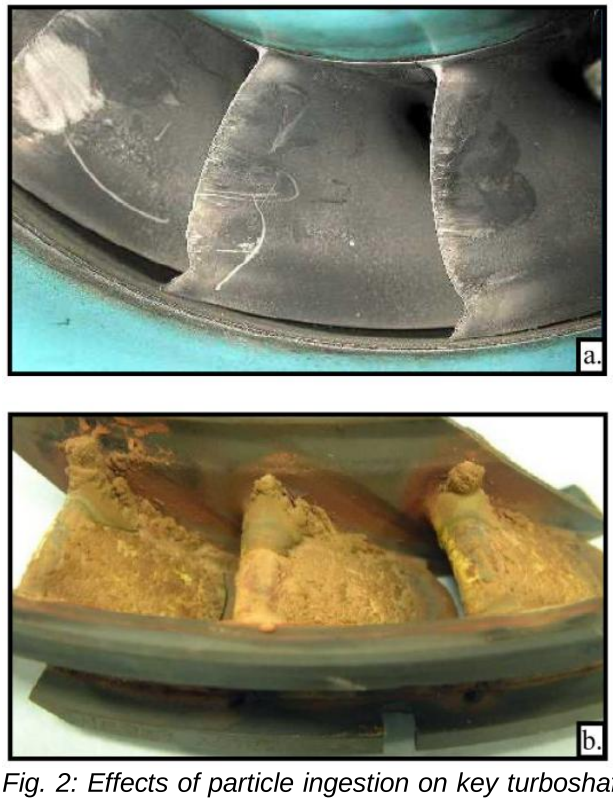

Fig. 2: Effects of particle ingestion on key turboshaft engine components, illustrating: a. leading and trailing edge erosion of compressor blades; b. agglomeration of molten impurities on turbine blades. (Images © Crown Copyright.)

Fortunately, since the first Gulf War there has been a great progress made in limiting this kind of damage, through the use of EAPS. For example, one study purports to achieve a hundredfold increase in mean time between overhaul as a result of using an inlet barrier filter[12]. However, as a particle's size diminishes, it becomes more difficult to remove. Van der Walt & Nurick studied degradation of an engine fitted with an array of vortex tube separators, focusing on efficiency of removal and subsequent fate of the unfiltered particulate[13]. Using a macroscale approach to the effects of erosion, they were able to predict engine lifetime by relating the resulting unfiltered particle size to the rate of metal erosion. Crucially, however, the interaction of unfiltered particulate on hot section components and the consequent effect on degradation was not considered.

The work presented herein reports the authors' progress in predicting engine performance loss and through life costs due to the degradation of turbine nozzle guide vanes and rotor blades by desert particulate. The blockage of cooling holes, one of the two main effects leading to turbine degradation, is predicted as part of the methodology.

2 BACKGROUND

Research on particle deposition in the hot section of turbomachinery has received more attention since the turn of the century. Initial motivation has been prompted by the deposition found on the surface of turbines of combined-cycle power plants using 'new' alternative fuels. In lieu of natural gas, these power plants use a filtered syngas generated from 'dirty fuels' such as coal, biomass and oil residue petcoke that contain trace amounts of uncaptured particulate. When this combines with the hot combustion products, the result is a gradual building up of deposits on the turbine vanes and blades. This has proven to be detrimental to component life, and authors are continuing research into mechanisms of deposition (Ref.[10, 14]). More recent attention on turbine degradation arose following the Eyjafjallajokull eruption of 2010, which highlighted the insufficiency of experimental data on accretion and sintering rates of ingested volcanic ash in the prediction of engine performance loss. This has prompted recent studies into the effect of ash ingestion on engine performance (Refs.[15, 16]); Davison & Rutke[11] provide a comprehensive review of much of the literature to date on the threat of volcanic ash to aircraft engines.

While ash composition is typically different to that found in desert dust, there is plenty of overlap in the techniques used to characterize and predict degradation, particularly concerning mechanisms of particle capture and locations of deposition. Volcanic ash typically contains compounds that transition to glass at relatively low temperatures (approximately ≤ 900°C). This exacerbates the deposition of ash particles by producing a sticky glass substrate on the blades into which higher inertia particles that would otherwise bounce may stick. While desert sand is mainly composed of high melting-point quartz, optical micrographs of leading edge deposits from four turbines operating in the Persian gulf[17] revealed similar deposition morphology: a glassy matrix containing second phase precipitates and even bright metallic by-products of upstream erosion. This suggests that the prediction of degradation by sand should carry a greater emphasis on contaminant mineralogy, as well as physical properties such as size and density as tends to be the case[18].

Particle deposition in hot section turbomachinery is a complex, multi-disciplinary process involving three-phase, time-variant flow. While little is still known about the effects of deposition, the literature on this subject is growing.

2.1 Particle Melting and Sticking Potential

As the ash or dust passes through the core of the engine, it can melt. The melting point for volcanic ash depends on silicate content and can be as low as 960 °C but is usually closer to 1100 °C[11]. The sticking potential of material at high temperatures has been recognized as a useful parameter to describe the likelihood of capture by hot gas turbine components[19]. According to Song et al.[16], a sticking-potential criterion requires consideration of:

a) The onset temperature at which the material is capable of sticking to a hot surface.
b) The time-dependent rheology of the ash as it evolves into a liquid.

The aim of these authors' work was to quantitatively characterize the fusion and sintering dynamics of volcanic ash with a view to determining the temperature at which a given sample gained the ability to stick to a surface. From the literature, they suggest that there are four characteristic temperatures in the phase transition of a material that describe sticking potential: the shrinkage temperature (ST), the deformation temperature (DT), the hemisphere temperature (HT), and the flow temperature (FT). They determined these temperatures by heating a cylindrically shaped volcanic ash compact (CSVAC) sample ash from Santaguito Volcano, Guatemala, from 50°C to 1400°C at a rate of 10°Cmin^{-1} and quantified the change in height, area and shape factor of the samples' silhouettes. The results depict an initially quadrilateral silhouette that begins to shrink at around 1100°C, becomes rounded at 1300°C resembling a liquid droplet attached under surface tension, then flows out to a half-dome at 1400°C. The shrinking can be attributed to sintering, and each of the temperatures above can be clearly recognised. The sintering phase is described as the temperature at which the area reduces by 1.5%, in this case determined as 1115°C; however, the samples only began to stick to the substrate once the sample had reached the deformation temperature (DT) (signified by the onset of sample edge rounding) at around 1250°C. The authors thus conclude that the sticking potential of volcanic ash becomes important once the temperature reaches the deformation temperature, which can be used as a temperature limit in assessing jet engine operation safety.

Whilst the sintering of many particles provides useful set of temperature markers for the agglomeration of deposits, it does not cater for the sticking ability of individual particles whose mineralogy will be distinct. Tafti et al.[20] developed a probabilistic sticking model based on particle viscosity, a property that changes with temperature and can be predicted from the properties of the material. Their work concerns deposition of coal ash on turbine nozzle guide vanes. They define a *critical sticking temperature* at which the material softens, and prescribe a probability of 1 for any particle of a given composition above this temperature. Particles with a temperature much below this have a probability of 0 whilst any other particle is assigned a probability of between 0 and 1 based on its temperature-dependent viscosity, and the viscosity at the critical sticking temperature of the material.

The temperature-viscosity relationship is determined using a series of empirical formulae that take the chemical composition (compound % by weight), as summarized by Barker[21]. Generally, a particulate melt will contain a balance of cations that act either as *glass formers,* which promote the formation of a glass structure, as *modifiers* that terminate chains in the structure, or as *amphoterics,* which can act as modifiers or formers. Modifier ions, such as Ca^{2+} or Mg^{2+}, disrupt the glass structure and tend to lower the viscosity. The temperature-viscosity relationship is reported in the same study for a number of different samples of ash, and appears to be linear. If one can ascertain the particle temperature, for example by knowing its heat transfer properties and residence time in the flow domain, then a *probability of adhesion* can be found from the calculated viscosity.

2.2 Particulate Composition and Concentration

From the above it should be fairly evident that the chemical composition of the ingested dust is as important as the physical properties for the prediction of erosion and deposition in turbomachinery. A study by Walsh et al.[22] investigated the effects of desert sand blockage in the cooling holes of a kiln-heated leading edge coupon. A reduction in coolant flow due to blockage by deposited materials was quantified using a flow parameter that is the ratio of momentum force to pressure force, as discussed by Hill[23]. They investigated the reduction in flow parameter for a range of parameters, including sand diameter and metal temperature. They found the latter to be the most significant parameter: as metal temperature increased beyond 1000°C, those particles not already molten either melted on impact or shortly after impact.

Walsh et al. used three test dusts as surrogates for real desert sand in the study. The samples were analysed to determine their chemical composition and size distribution, and heated to determine melting point. A bulk powder spectrum revealed that the test dusts were crushed granite, containing: 68-76%wt quartz (SiO_2) of varying phase; between 10-15% aluminium oxide (Fe_2O_3); and traces of iron oxide (Fe_2O_3), sodium silicate (Na_2O), lime (CaO), magnesium oxide (MgO), titanium dioxide (TiO_2), and potassium oxide (K_2O). While this gives an impression of the elements present in the sample, the mineralogy (i.e. crystalline structure) of the particle would be required to directly infer melting points. Instead, by baking a small sample of the test dust from 930°C to 1090°C, the sample began to show signs of melting by agglomerating at 980°C. By 1040°C a significant colour change was observed, and by 1090°C the now darker sample had become a solid block. Using this result and assuming adiabatic heating solely by radiation, the authors calculated that over a period of just 0.01s – a conservative residence time for a particle in the heated coupon – the particle would increase from 675°C to 820°C, based on a metal temperature of 1010°C. Given that the internal blade cooling channels are serpentine by nature, the particles may bounce and take a lot longer to exit the blade through the cooling holes than the air, by which time they may have reached melting point.

The proximity of the sand melting point to the typical turbine inlet temperature was thus one of the main causes of the substantial damage suffered by desert-operating helicopters in the past, as reported earlier. The investigation by Walsh et al.[22] was prompted by evidence of large quantities of sand being entrained into the compressor of C-17 engines. Unlike C-17 aircraft, helicopters can be protected by one of a range of EAPS devices[24]. Their use substantially changes the composition of the particulate that does happen to evade capture and reach the engine components. Physically, the uncaptured particulate has a much smaller mean diameter: in the aforementioned study by Van der Walt & Nurick[25], the mean diameter of the AC Coarse test dust that evaded removal by vortex tubes was found to be 4.9µm (from an original mean diameter of 38µm). Chemically, the uncaptured particulate has a much different mineralogy too: in the aforementioned study by Smialek et al.[8], powders and deposits found within Blackhawk T700 engines were found to resemble a fine dust silicate-based dust with much higher amounts of calcium, aluminium, iron, magnesium and carbon oxide species than ordinary dune sand from the same region. It is significant to note that these T700 engines are fitted with an inertial particle separator, which is effective at removing most particulate above 20µm.

The same study by Smialek et al.[8] referenced a prior study by Bessee & Kohl[17] conducted for the US Army in 1993, in which a number of soil samples were collected from various geographical areas on the Continental United States (CONUS) and Saudi Arabia. Their aim was to characterize each sample using particle size distributions, elemental analysis, mineral composition, and particle angularity, to determine whether new test dusts used to evaluate fuel filters for land-based vehicles were representative of naturally occurring soils. 22 samples were examined and generally fell into three families: *a. high calcium, no silicate; b. magnesium silicate; and c. high silica*. Only a limited amount of the sand samples matched standardized test dust compositions (including AC Coarse and AC Fine test dusts, used respectively in the studies by Walsh et al.[22] and Van der Walt & Nurick[25]). In a separate contribution but using the same samples from the fouled Gulf War T700, Smialek et al. compared the chemical composition of one such Saudi sample with deposits found in cooling holes and nozzle guide vanes, as shown in Fig. 3[26]. While it is not known just how much quartz passes right through the engine, these results indicate a vast difference in composition between the dust on the ground and the dust reaching the engine components.

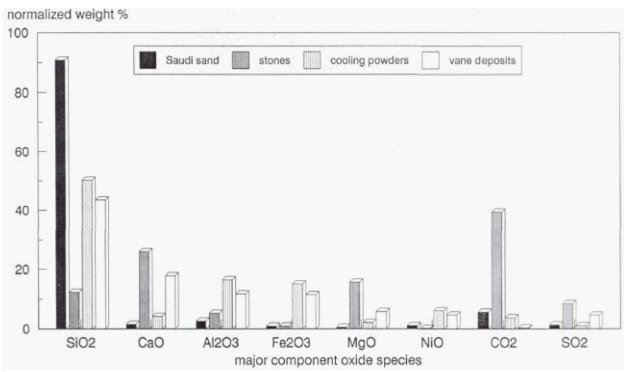

Fig. 3: Analysed composition of Saudi Arabian sand and helicopter engine deposits. (Presented as oxide species normalized to 100% total.) Averages of cooling passage powders and vane deposits from 4 engines). Major components.[17]

As well as differing in chemical composition, the 22 samples analysed by Bessee & Kohl exhibited different particle size distributions (PSD) from one location to the next. This is expected, given the great variability of geology across the globe. However, the study also found variation in PSD of airborne particulate with height above the ground. To test this, a light armoured vehicle (LAV) was driven along a dirt road past a 3-metre pole with an array of sampling containers. As can be imagined, there was a greater abundance of sub-10µm particles in the highest placed containers due to their lower terminal descent speed. In addition, a spike in total mass collected was found in the container at 1.5m, assumed to be the result of air currents generated by the vehicles.

A similar experiment was performed as part of the Sandblaster 2 study by Cowherd et al.[27] in 2007, which aimed to develop quantitative field information for rotary wing and tilt rotor aircraft dust clouds to help evaluate new 'see-through technologies' for use in brownout operations. Using a similar approach to that described by Bessee & Kohl, their report gathered data relating to*: a. dust cloud densities and particle size distributions; b. spatial distributions (heights, distances from rotors); and c. relationship of dust cloud densities to downward rotor force*. No data on the chemical composition of the samples taken are available in the open literature. A number of vertical lift aircraft with intentionally contrasting downwash signatures were tested. In addition to illustrating a variation in particle size with height, the results showed that each aircraft creates a unique brownout cloud exhibiting differences in dust concentration and size distribution. The results are shown in Fig. 4.

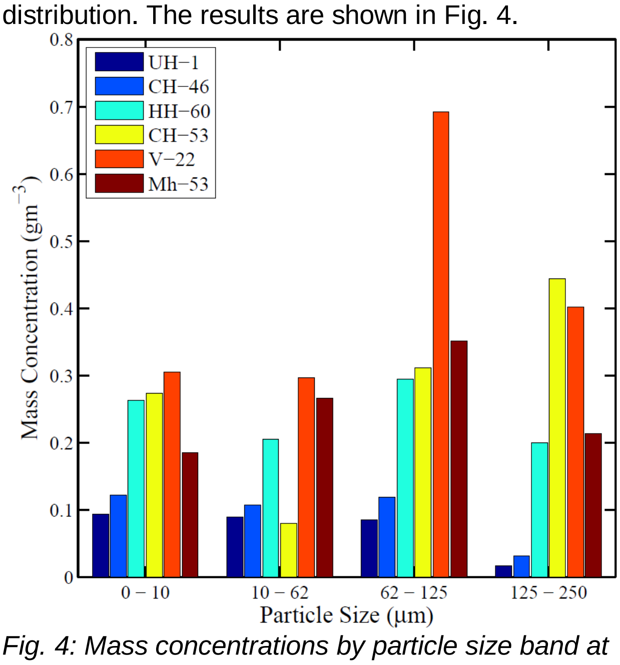

Fig. 4: Mass concentrations by particle size band at the rotor tip location for six rotorcraft, as taken from Sandblaster 2 tests[27]*.*

In Fig. 4 one can see that from the data pertaining to the HH-60 there is an almost equal mass concentration of particles in the 0-10µm range as all other size bands, while the CH-53 produces a relatively low concentration of 10-62µm particles but a high concentration of larger particles in the 125-250µm range. The differences are related to the unique upwash mechanisms created by each main rotor downwash – a complex mix of merging detached tip vortices and strong groundwash jets. Attempts have been made to at least qualitatively relate the brownout signature to the rotor design parameters (Refs.[28], [29]), but quantitative results are limited. Nevertheless, the Sandblaster 2 results suggest that consequent degradation rates may be a function of the aircraft within which the engine is installed. Incidentally, the Sikorsky HH-60 uses a GE T700 turboshaft to provide power to the rotor system.

The above should begin to highlight the complexity of developing a suitable methodology for predicting engine degradation that encapsulates all the contributory parameters.

2.3 Particle Transport and Deposition

If a particle evades removal by the EAPS system, its journey through the engine will depend upon its diameter, shape, density, as well as properties of the carrier fluid, all of which can vary due to temperature and pressure changes.

Once beyond the EAPS system, an ingested particle will continue with the main flow to the compressor stages, which it will most likely pass through and reach the combustor. A very small percentage may become attached to surfaces of the compressor through van der Waals force (the dominant sticking force for non-molten particles) while a larger percentage may enter the bleed line and head towards the turbine blade cooling passages. The mass of bleed air for turbine cooling varies, but is typically 3-5% of the inlet mass flow[30]. As mentioned in Hill et al.[23], even small gas turbines such as the General Electric T700 are amenable to internal blade cooling. The cooling air is split between the nozzle guide vanes and rotor blades of the high pressure turbine, initially following serpentine multi-pass channels within the blades before exiting through a number of small holes to re-join the core flow. The exit holes vary in their orientation to the oncoming core flow, but are designed to create a thin layer of cooler air around the blade to absorb some of the heat from the core flow and permit the blades to operate in temperatures beyond their stress limit. For more details of typical internal cooling channel and film-cooling hole arrangement, see Han et al.[30].

Such a tortuous path in an increasingly hot environment presents many opportunities for the particle to become attached to a surface. If the viscosity of the particle dictates a high probability of sticking, the particle may do so on the exit of a bend of an internal cooling passage, or as it negotiates a sharp change in direction to pass through a hole in the turbine wall. This capture mechanism is known as inertial impaction. Several investigators have devised experiments to simulate the effects of particulate deposition within cooling passages; a recent review is given by Singh et al.[18]. Walsh et al.[22] subjected a 60-hole and a 36-hole coupon, kiln-heated, to cooling flow containing concentrations of ISO Coarse and ISO fine test dusts, under different operating conditions. They found that the rate of deposition was proportional to the coupon casing temperature, particulate concentration, and particle size, and found to be inversely proportional to the pressure ratio.

The problem is complicated by the inherently turbulent nature of the flow, which may be added to by the addition of channel ribs designed to augment heat transfer. These secondary flows create rotating eddies that can entrain low Stokes number particles outside of the wall boundary layer and deposit them on the channel wall[18]. This capture mechanism is known as eddy impaction. Two other capture mechanisms present as described by Hamed & Tabakoff[9] are: turbulent diffusion, whereby particles within the turbulent boundary layer can be swept towards the wall by turbulent eddies; and thermophoresis, whereby sub-micron particles are bombarded by thermally agitated gas molecules and transported to the wall by impact force. Brownian motion is a similar mechanism that may cause a particle to change direction and impact a wall.

Thermophoresis is more applicable to deposition from the core flow or film coolant to the blade surface, which is cooler. Surface deposition is found to be much more prevalent a problem, in some cases resulting in thick amorphous agglomerations up to 6 mm thick[26]. Almost all of the recent experimental and numerical investigations in the open literature on this subject are based on synthetic-fuel powered gas turbines for power generation (Refs.[10], [14], [20], [31], [32]). In research by Bons et al.[33], the increase in surface roughness due to deposition was found to increase heat transfer by up to 50% skin friction by up to 300%[33], [34]. The effectiveness of the film cooling is also adversely affected as it is influenced by the morphology of the deposit in the vicinity of the cooling holes.

The deterioration process is almost always non-linear, since the reduction in cooling effectiveness leads to a hotter blade that accelerates the sticking process. Furthermore, studies of deposit growth behavior suggests that entrained particles more readily adhere to surfaces that have some initial deposit coverage, as opposed to clean surfaces[10]. In all cases the deposition was seen to increase with surface temperature, growing faster in between cooling holes and not in the cooler surface temperature region in the cooling flow channels. In some cases the cooling hole may become completely blocked, which can have disastrous consequences. Surfaces coated with a thermal barrier coating generally encourage more sticking due to their outer surface running hotter, although the blade itself is cooler. The relationship between parameters such as hole spacing, hole shape, coolant blowing ratio, and vane/blade geometry on deposition mechanics represents the most recent developments in the literature, as researchers look for ways to mitigate damage and prolong component life.

3 PROPOSED METHODOLOGY

From the evidence presented in the preceding section, a picture emerges of the complexity of modelling engine degradation due to sand ingestion. Even characterizing the dust that enters the helicopter engine is a multi-variable problem. Once ingested, the likelihood of particle deposition is dependent on its own mineralogy and Stokes number, while the morphology of the resulting surface agglomerate depends on the overall physical and chemical properties of the adhered particulate and surrounding flow conditions. The consequence of deposition is a blocking of cooling holes and reduction in core flow area.

While separate research has been reported on desert sand characterization, on particle heating, and on the effects of deposition on heat transfer at the blade, all with respect to turbine degradation, to the authors' knowledge no studies on predicting the macro-scale consequences on engine performance have yet been reported in the literature. To deal with the multitude of contributory parameters, a methodology is proposed that takes a multi-block, gas-particle path analysis approach to modelling the effect of sand ingestion on helicopter engine performance. This is depicted in Fig. 5.

3.1 Ingestion Model

The first objective is to ascertain the properties of the particulate reaching the engine during a brownout landing, and the rate at which those particles are ingested.

3.5 Particulate Mass Flow Rate

The Sandblaster 2 study revealed a variation in the size distribution and concentration of particulate surrounding the airframe[27] and intimated a link between dust concentration and disk loading but provided no empirical relationship. The sediment uplift is thought to be a combination of two mechanisms created by the rotor wake. A groundwash jet creates a surface boundary layer that liberates particles form the surface, while impinging detached tip vortices loft the particles higher into the air. Assuming the groundwash jet is always large enough to release particles, it follows that a higher and stronger vortex impingement rate will result in a fast-forming, dense dust cloud. However, a large downwash resulting from a high disk loading may push airborne particulate away from the helicopter before it can be lifted into the air by tip vortices.

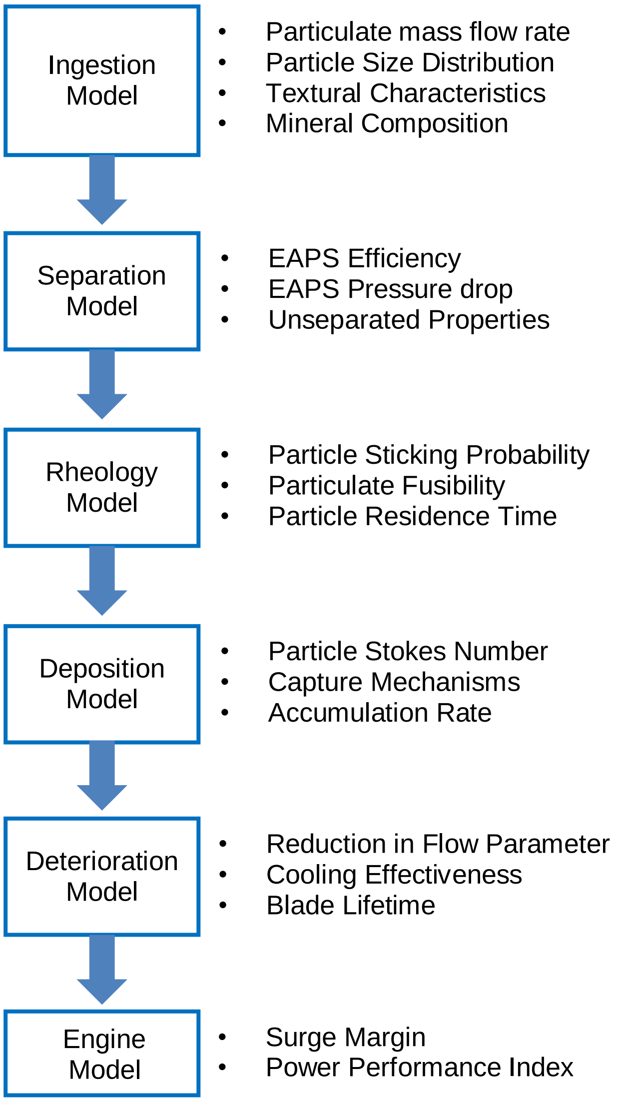

Fig. 5: Multi-block approach to macroscale modelling of engine degradation by sand ingestion.

In quantifying these features, Milluzzo & Leishman[28] attempted to relate the brownout severity level to: *a. Total Wake Strength*; *b. Wake Vortex Impingement Rapidity*. The wake strength gives a measure of the intensity of the brownout cloud, and is defined quantitatively as a product of the tip vortex strength Γ_v and the total number of blades N_b, normalized with $\Omega_R {R_R}^2$. The tip vortex strength can be approximated as a product of the blade loading coefficient C_T/σ, tip speed $\Omega_R R_R$, and blade chord c_b. Hence, the normalized total wake strength, Γ_w^* can be written:

(1) $$\Gamma_w^* = \frac{N_R N_b}{\Omega_R R_R^2}\Gamma_v \approx k N_R N_b (C_T/\sigma)\frac{\Omega_R R_R c_b}{(\Omega_R {R_R}^2)}$$

Where Ω_R is the rotational frequency, R_R is the rotor disk radius, N_R is the number of rotors, C_T is the thrust coefficient, and σ is the rotor solidity. k is an empirical constant equal to 2 in hover (from vortex theory). The rate of production is related to the frequency of vortex impingement on the ground, and is called the *wake convection frequency*, Ω_s given by:

(2) $$\Omega_s = N_R N_b \Omega_R$$

From this relationship one can see that a helicopter with a greater number of blades and/or higher rotor rotational speeds may tend to uplift more sediment from the ground per unit time, all other factors being equal. This can be used to establish a quantitative brownout metric by establishing a reduced frequency, defined as:

(3) $$k_s = \frac{\Omega_s c_b}{2\Omega_R R_R}$$

And comparing it with the normalized total wake strength Γ_w^* and the normalized downwash, defined as:

(4) $$w^* = \frac{w}{\Omega_R R_R}$$

Where w is the slipstream flow velocity. When calculated, these values allow a particular helicopter to be rated in terms of its brownout characteristics. Based in its rotor design, a helicopter is assigned a level of 1 to 3 for each of the above metrics. These levels are based on anecdotal (videographic) evidence of large set of existing helicopters entering a brownout landing.

While it is acknowledged that this approach is macroscale and does not account for many other contributory factors such as blade tip shape, blade twist, and local dust type, it can be crudely used to suggest a dust concentration based on experimental data. For example, from the Sandblaster 2 experiment (Ref.[27]), the V-22 was found to create a mean volume concentration of 1.62 gm^{-3} at the rotor tip. As a Level 3 rotorcraft according to Milluzzo & Leishman, this could be used as a benchmark concentration for all other Level 3 rotorcraft. However, the concentration at the rotor tip does not necessarily correlate to the concentration at the intake; more work is required in this area.

If the concentration is at least estimated (other technologies exist to directly measure dust cloud density), the particulate mass flow rate into the engine, $\dot{m}_p$ is a simple calculation:

(5) $$\dot{m}_p = c_m \dot{m}_a$$

Where $\dot{m}_a$ is the engine mass flow rate and c_m is the particulate concentration by mass. With reference to the Sandblaster 2 study, dust cloud densities are usually quoted as a volume concentration, i.e. mass of particulate per unit volume of carrier fluid. The conversion to mass concentration is found by considering each phase's density and volume, and is expressed as:

(6) $$c_m = \frac{1}{\rho_g/c_v + (1-\rho_g/\rho_p)}$$

Where ρ_g is the gas density, ρ_p is the particle density, and c_v is the volume concentration.

3.1.2 Particle Size Distribution

Particle size distribution (PSD) is one of the more difficult variables to determine. By performing a variety of sieving techniques on a sample, one can establish the PSD of a given area of operation as a starting point. To determine what proportion of the size distribution reaches the engine inlet is more difficult, as the upwash mechanisms may not be powerful enough to loft all sizes of particles to a height at height they can be intercepted by the engine. Since most engines are located directly below the rotor disk, any particulate that reaches the engine has probably been re-ingested by the rotor disk. The *recirculatory mode* is one of the stages of a brownout landing identified by Phillips et al.[35], which happens at low forward speeds and can result in the formation of a large vortex at the rotor disk leading edge, causing an appreciable portion of the flow near to the ground to be re-ingested through the forward portion of the rotor. Only particles with a low enough Stokes number will remain entrained in this vortex, hence through this process, the ground sediment undergoes a rather rudimentary form of centrifugal separation.

Characterising that separation is simplified here by assuming that the mean vortical flow has a tangential velocity equal to the average induced velocity v_i, which through classic momentum theory for a hovering rotor can be found from rotor design parameters as:

(7) $$v_i = \sqrt{\frac{T}{2\rho_g A_R}} = \sqrt{\frac{DL}{2\rho_g}}$$

Where T is the rotor thrust (approximately equal to rotorcraft weight), A_R is the rotor disk area, and DL is the disk loading.

The particle size distribution is most usefully presented as a percentage by mass of a number of representative sizes. Typically, some form of sieving (the exact technique depends on the size; smaller sizes for example can be susceptible to inter-particle forces that influence results) will be used to determine the mass of particulate 'no smaller than' a given mesh size. Occasionally the size distribution may be expressed as number of particles per size band. In that case, a simple calculation can convert to mass fraction:

(8) $$m_{p,i}^{+} = \frac{k_{v,i} d_{p,i}^3 \rho_{p,i} f_i}{\sum k_{v,i} d_{p,i}^3 \rho_{p,i} f_i}$$

Where $d_{p,i}$ is the characteristic diameter of the ith size band range (usually the mid-point), ρ_i is the mean density of the ith size band, f_i is the number of particles in the ith size band, and $k_{v,i}$ is the mean volume shape coefficient of the ith size band.

The size distribution can be represented by an arithmetic mass mean diameter, $\bar{d}_p$, and an arithmetic standard deviation, σ_p:

(9) $$\bar{d}_p = \sum_{i=1}^{N_p} d_{p,i} m_{p,i}^{+}$$

(10) $$\sigma_p = \sqrt{\sum_{i=1}^{N_p} m_{p,i}^{+} \left(d_{p,i} - \bar{d}_p\right)}$$

Where N_p is the number of size bands. This information allows a more generalized distribution to be found. Dust sample in nature are commonly found to exhibit a log-normal distribution that can be represented by a probability density function of the form:

(11) $$\mathrm{PDF}\left(x, \bar{d}_p, \sigma_p\right) = \frac{1}{x\sigma_{p,3}\sqrt{2\pi}} \exp\left[-\frac{(lnx - \bar{d}_p)}{\sigma_p\sqrt{2}}\right]$$

This is a well-known distribution, whose characteristics are given in several mathematics textbooks.

3.5 Textural Characteristics

The textural characteristics essentially encompass the angularity and sphericity of the particle, which influence the particle drag coefficient. The sphericity is a measure of how compact the volume of an object is. It is defined as the surface area of a sphere with the same volume as the particle, divided by the actual surface area of the particle:

(12) $$\psi = \frac{A_s}{A_p} = \frac{\pi^{\frac{1}{3}}(6V_p)^{\frac{2}{3}}}{A_p}$$

Where A_p is the surface area of the particle, A_s is the surface area of a sphere of equivalent volume to the particle, and V_p is the volume of the particle. Angularity is more qualitative by nature, and is used as an indicator of a particle's abrasion history, hence is more a measure of the particle's roundness. However, it can be used to infer the skin friction coefficient of a particle.

The two characteristics are not the same, as a rounded particle may be flat thus have low sphericity, while a dodecahedron-shaped particle may have high sphericity but may be considered angular. The sphericity is used to define a volume shape coefficient, k_v, as featured in Eq. (8) as follows:

(13) $$k_v = \frac{\pi \Psi^{\frac{3}{2}}}{6}$$

A derivation is provided in Bojdo, Ch. 3.2.3[36]. For example an angular particle with $\Psi = 0.54$ (qualitatively termed 'flaky') will have a volume shape coefficient of $k_v \approx 0.28$. Similarly, a spherical particle with $\Psi = 1$ yields a shape coefficient of $\pi/6$, as expected for the calculation sphere volume.

3.1.4 Mineral Composition

The chemical composition has been classified via a number of techniques: atomic emission and absorption spectroscopy, x-ray crystallography (commonly known as XRD), scanning electron microscope, differential thermal analysis, metallography. Atomic emission and absorption spectroscopy can be used to determine the minerals present in a given sample and determine the elemental composition of given particle. Using XRD, one can infer the crystallographic structure of the mineral to inform how the elements are chemically bonded. For example, high levels of silicon and oxygen from the elemental analysis indicate that the material is a silicate mineral, while a three-dimensional tetrahedral crystal framework may indicate the silicate family, such as quartz. Within the silicate family, there can be several forms of the same mineral. Each of these branches can result in a different melting point, hence it is important to determine the mineralogy of the sample as well as the physical properties.

3.2 Separation Model

Once at the engine inlet, the particles are met by an EAPS system, as is common on all rotorcraft operating in the desert nowadays. The EAPS systems differ by the removal mechanisms they employ: Inlet Barrier Filters arrest particles on their surface; Vortex Tubes swirl the flow to centrifuge particles to an annular scavenge chamber; while a hump attached to the engine works as the vortex tubes but axially, in an Integrated Inertial Particle Separator. The latter two inertia-based separators require extra mass flow to operate.

3.2.1 EAPS Efficiency

The efficiency of an EAPS system depends on a number of parameters, including particle Stokes number, device geometry, scavenge mass flow rate. For a comprehensive discussion see Ref.[36]. Assuming the device is working at a design point, it will have a *grade efficiency* expressed as a function of particle size, $E_{EAPS}(x)$. For the present work, however, it is the particulate that evades capture that is of interest. The PSD of the ingested particulate is related to the size distribution calculated in Eq. (11):

(14) $$f(\phi) = \left(1 - E_{EAPS}(x)\right)\mathrm{PDF}\left(x, \bar{d}_p, \sigma_p\right)$$

Where ϕ is the ingested (unseparated) particle diameter.

3.2.2 EAPS Pressure Drop

The pressure drop, similar to the efficiency, is a function of the device geometry and flow conditions. Analytical expressions exist to predict the pressure loss across vortex tubes and barrier filters, but it is more difficult to similarly predict for integrated particle separators. Inlet barrier filters typically begin with a pressure loss of around 0.54%, rising to 2.97% as dust accumulates. An analytical study by the authors revealed a low pressure loss across a typical vortex tube of around 0.42%, although this only considered skin friction drag; a more realistic approximation would be double this. A CFD simulation of an integrated particle separator by Taslim & Spring revealed pressure losses of up 0.96%[7]. A study by Bojdo & Filippone revealed that in all cases the pressure loss was a function of the mass flow rate, with the integrated separator rising steepest with mass flow rate[1].

3.2.3 Unseparated Particulate Properties

To enable the prediction of engine damage by ingested particulate, the size distribution calculated in Eq. (14) can be used. As this represents a probability density function, the mean diameter of the contaminant is simply:

(15) $$\bar{\phi} = \int_0^1 \phi f(\phi) d\phi$$

Smialek et al.[8] found that the unseparated particulate not only had a narrower and smaller size distribution than the ground sediment PSD, but also a different chemical composition (see Fig. 3). A significant reduction in quartz content was found. This suggests that the smaller sized particles in the sample are dominated by other minerals, which may decrease the overall deformation temperature (DT) discussed in Section 2.1, at which the particulate begins to stick. It would be useful therefore to explore further the change in particulate mineralogy as the particle size distribution is modified post-filtration.

The mass flow rate of unseparated particles is calculated in a similar way, by calculating the mean separation efficiency, $\bar{E}_{EAPS}(x)$ and multiplying it by the particulate mass flow rate given in Eq. (5):

$$\dot{m}_{\phi} = (1 - \bar{E}_{EAPS})\dot{m}_p = \left(\int_0^1 f(\phi)d\phi\right)\dot{m}_p \tag{16}$$

This is useful as it gives the true rate at which particulate enters the engine, in spite of an EAPS system being in place.

3.3 Rheology Model

The rheology model determines the likelihood of a single particle adhering if it comes into contact with a surface. It also determines the temperature at which the particulate as a whole begins to agglomerate and potentially glaze.

3.3.1 Particle Sticking Probability

The sticking probability of a single particle is related back to its mineralogy. It bridges the gap between the particle melting point, and the solid, as there exists a small range of temperatures during which the particle may be soft enough to stick on impact. This is more common in ash, which has more particles that undergo glass transition, but is applied here to create a general case.

A viscosity sticking model is proposed by Barker[21] which draws on a number of authors' work. First, a critical softening temperature is defined, T_s. Particles above this have a sticking probability of 1. Particles much below this have a probability of zero. For particles in between, the probability function is:

$$\mathrm{PDF}(T_p) = \frac{\mu_{crit}}{\mu_{T_p}} \tag{17}$$

Where T_p is the current particle temperature, μ_{crit} is the viscosity at the critical sticking temperature, and μ_{T_p} is the viscosity at the current particle temperature. The temperature dependence of viscosity of silicate and aluminosilicate melts can be described by the following empirical relationship:

$$\log\left(\frac{\mu_p}{T_p}\right) = A + \frac{10^3 B}{T_p} \tag{18}$$

Where A and B are constants that depend on the chemical composition, or more specifically the balance of *amphoterics* and *modifiers* as described in Section 2.1. The ratio of non-bridging oxygens to tetrahedral oxygens, (NBO/T) is:

$$\frac{NBO}{T_p} = \frac{\{CaO + MgO + FeO + Na_2O + K_2O - Al_2O_3 - Fe_2O_3\}}{0.5(SiO_2 + TiO_2) + Al_2O_3 + Fe_2O_3} \tag{19}$$

Where the terms on the right hand side represent the chemical formulas of the minerals present. The constant A varies with (NBO/T) while both A and B are determined for two temperature regions (low and high) and are determined by curve fitting experimental results. The product is a relationship between temperature and viscosity in the two regions; the higher of the two is adopted by Barker.

3.3.2 Particle Residence Time

In order to apply the previous relationship, an estimate of the particle temperature is required. As it travels through the compressor, the particle's temperature can be assumed to rise in proportion to the gas temperature. A small portion of the particulate-laden flow is bled off the compressor to the internal cooling channels of the compressor blades, at which point the flow experiences a sudden increase in temperature, especially within the wall boundary layer. Conversely, particles that pass all the way through the combustor and arrive at the turbine blades may interact with a region of film cooling and undergo a sudden decrease in temperature.

To model sudden changes in heat transfer to a particle, a simple lumped mass approximation is adopted. Consider the case of particles in the cooling holes. Initially particles are at the temperature of the compressor stage at which the coolant was bled, T_i. The ambient gas temperature is T_∞. The particle temperature as a function of time is given as:

$$T_p(t) = T_\infty + (T_i - T_\infty)e^{-bt} \tag{20}$$

Where t represents residence time and b is the time constant. The time constant is dependent on properties of the particle and the heat transfer coefficient, h:

$$b = \frac{hA_p}{\rho_p V_p c_p} \tag{21}$$

Where A_p is the particle surface area, V_p is the particle volume, and c_p is the specific heat capacity at constant pressure of the particle. The heat transfer coefficient, h, can be approximated from the analytic solution for conduction from a sphere.

The specific heat capacity at constant pressure is assumed to be equal to the value at constant volume, and can be found by looking again at the chemical composition of the particle. The specific heat capacity is estimated by adding the Kopp value heat capacities of the constituent atoms. For example, silicon has a heat capacity of 15.9 Jmol-

$^{1\circ}C^{-1}$, while oxygen has a heat capacity of 16.7 $Jmol^{-1\circ}C^{-1}$, which means the heat capacity of quartz (SiO_2) is estimated as 49.3 $Jmol^{-1\circ}C^{-1}$. Magnetite, a mineral also found in desert samples, by comparison has a heat capacity of 143.5 $Jmol^{-1\circ}C^{-1}$.

3.3.3 Particle Fusibility

The tendency for deposited particulate to fuse is also included in the rheology model. As single molten particles stick to turbine surfaces and form a deposit, the surface temperature can rise due to inefficient cooling. The individual particles may begin to agglomerate and form a coherent mass that may stick more solidly to the turbine blade and insulate the blade more thoroughly. Davison & Rutke[11] predicted the deformation temperature (DT) to be the critical point at which particles under pressure begin to sinter and exhibit more fluid-like properties. A number of other key temperatures were identified in the heating process that could help to define the evolution of the deposited material, although more work is required in this area. An initial step would be to follow the procedure set by Davison & Rutke.

3.4 Deposition Model

The rheology model and deposition model are interdependent: the particle trajectory through the complex domain dictates the residence time hence particle temperature, and ultimately where the particle will stick if it meets the sticking criteria. Likewise, as particles buildup, the flowfield and heat transfer between the fluid and the blade are affected, which then influences the particle trajectory and rheology, and so on.

3.4.1 Particle Stokes Number

The Stokes number can be used to determine how the fluid and inertial forces will influence the motion of a particle. The Stokes number is a non-dimensional parameter that represents the ratio of particle response time to domain fluid response time. The particle response time, or how fast the a particle reacts to the fluid forces imposed upon it, can be determined by the ratio of the effective particle momentum to the acting fluid forces:

$$St = \frac{\tau_p}{\tau_g} = \frac{\rho_p d_p^2}{18\mu}\frac{u_g}{D} \qquad (22)$$

Where τ_p is the particle response time, τ_g is the fluid response time, u_g is the fluid bulk velocity, and u_g is the characteristic domain length, e.g. hydraulic diameter. If a particle's response to the fluid is dominated by its own momentum forces, its response time to a change in direction, for example, will be longer than the fluid response time, resulting in a Stokes number greater than 1, and vice versa. A particle whose Stokes number is around unity is likely to have its motion affected by both bouncing and fluid forces[3].

The particle shape in a given sample will vary considerably, which means each has a unique drag coefficient. It would be impossible to model this, so without lack of generality the characteristic particle diameter is that also implemented into Eq. (11).

The typical forces acting on a particle are drag, gravitational forces, the Saffman lift force due to shear of the surrounding fluid, added mass, pressure and viscous forces, Bassett forces due to fluid acceleration, Magnus lift force due to particle rotation, forces due to particle rotation, and if the particle is sub-micron in size, thermophoretic forces and Brownian motion. For the size range of particles that are likely to enter the engine i.e. 0.5-25 μm, (see Ref.[8]), and considering the high density ratio of dispersed to carrier phase, the only significant forces are drag and gravitational forces[18]. Under these assumptions, the simplified equation of motion of a particle is given as:

$$\frac{du_p}{dt} = -\frac{\rho_g}{\rho_p}\frac{3}{4}\frac{C_D}{d_p}\left|u_p - u_g\right|\left(u_p - u_g\right) \qquad (23)$$

Where u_p is the particle velocity, u_g is the carrier (gas) velocity, d_p is the particle diameter, ρ_g and ρ_p are the gas and particle densities, and C_D is the drag coefficient.

Accurate models exist to predict the drag coefficient, including those for non-spherical particles that employ a shape factor as calculated in Eq. (13), such as the model by Haider & Levenspiel[37]:

$$C_D = \frac{24}{\mathrm{Re}_p}\left(1 + b_1 \mathrm{Re}_p^{b_2}\right) + \frac{b_3 + \mathrm{Re}_p}{b_4 + \mathrm{Re}_p} \qquad (24)$$

Where the coefficients b_i are a function of shape factor, and Re_p is the particle Reynolds number, defined as:

$$\mathrm{Re}_p = \frac{\rho_g (u_p - u_g) d_p}{\mu} \qquad (25)$$

Eq. (24) is valid for Reynolds numbers below 10^5.

3.4.2 Capture Mechanisms

When the particle is in the vicinity of the wall, it may experience forces that attract it closer to the wall and retain it there. Of the four mechanisms described by Hamed & Tabakoff[9] described in Section 2.3, inertial impaction is the most important for particles in the range of 0.5-25μm, whereby a particle impinges a surface by virtue of its momentum. If a particle's trajectory takes it close to the wall, it may impinge the surface by virtue of its bulk; this is known as direct interception and like inertial impaction, depends on the particle Stokes number.

In most recent CFD studies on particle transport in blade cooling holes and turbine nozzles, particles are tracked in a Lagrangian framework (Refs.[18], [21], [38]). If a particle trajectory impinges a wall, its collision is assigned as either perfectly elastic (bounces) or perfectly inelastic (adheres). The sticking probability model outlined in Section 3.3.1 aims to create an intermediate condition, but ultimately the process of deposition depends on many factors and may require a case-specific empirical model, such as in Ref.[38].

3.4.3 Accumulation Rate

It follows that if deposition can be modelled, then it may be possible to predict the gradual accumulation of a surface deposit that is large enough to significantly influence the flowfield. An accumulation model is difficult to derive analytically, as the location of particle build-up may vary with flow conditions, pressure ratio, particle properties and so on. The situation is more conducive to a numerical solution, as has been attempted in the literature[18], [21], [38]. However, these authors did not model the effect of accumulation on the flow. Modifying a computational mesh in such small increments as to capture individual particle deposition is likely to be extremely computationally heavy.

A novel Computational Fluid Dynamics (CFD) simulation is proposed that models turbine cooling hole blockage. The cooling hole geometry is initially discretised with a structured mesh, with high cell density at the wall. A quasi-steady state solution is solved, whereby particles are tracked in a Lagrangian framework, then updates to the flow domain are made based on any particle interactions with the wall and thermal boundary layer. The particle's temperature is updated along the trajectory and its subsequent sticking probability, as calculated in Section 3.3.1 is monitored. If the sticking probability reaches unity, its path is terminated upon collision with a wall. If the probability is zero, the collision is considered elastic. For probabilities between zero and unity, a random number generator provides a number between 0 and 1; if the random number generated is greater than the probability of sticking, the particle reflects off the surface. It follows that higher particle temperatures will have higher probabilities of sticking, as the gap into which the random number can fall decreases. This approach is adopted from[21].

If a particle is deemed to have adhered, its location, physical properties and chemical properties are recorded, along with the cell ID of the location. Ideally that cell would resemble the shape of the impacted particle and could be designated as solid. However, the smallest cell size will still be larger than the particle size. Instead, the cell's permeability and porosity is decreased to imitate the resistance to flow caused by the presence of the particle. When the cell's porosity becomes zero, it is designated as solid and influences the flow accordingly. After each deposition 'cycle', in which all particle collisions have updated their respective host cells, the flowfield is updated and the process repeated. This approach allows for the gradual accumulation of particulate on the walls of a cooling hole to be modelled, and has been applied successfully in a similar way by Fotovati et al.[39] to model particle build-up on a pleated filter. It allows the temporal reduction in mass flow or increase in pressure loss to be found as a function of particulate concentration and other flow conditions. Since the work is in a nascent stage and is yet to be verified, results are not presented here.

3.5 Turbine Deterioration Model

The deterioration of the turbine due to the two locations of deposition results in three main effects:

a. Increase in overall blade temperature.
b. Reduction in nozzle area.
c. Loss of pressure across stage.

To compute these effects and gain a picture of overall engine degradation, the following parameters are determined.

3.5.1 Reduction in Flow Parameter

The gas turbine industry generally uses a term called *flow parameter* (FP) for overall estimates of coolant flow supplied to a particular airfoil. The flow parameter is a non-dimensional term that is the ratio of momentum force to pressure force, as discussed by Hill et al.[23]:

$$\text{FP} = \frac{\dot{m}_C\sqrt{T_{oc}R}}{P_{oc}{D_c}^2} \tag{26}$$

Where $\dot{m}_{oc}$ is the coolant mass flow rate, T_{oc} is the coolant total temperature, R is the gas constant for air, P_{oc} is the coolant total pressure, and D_c is the cooling hole diameter.

Walsh & Thole[22] state that when the engine flow parameter and temperatures are matched to realistic engine conditions, the residence time of the air in a component will match the residence time in the airfoil component during operating conditions, even if the pressure ratio is not matched. For a particular airfoil at a given coolant temperature, there exists a clear relationship between the flow parameter and the pressure ratio. The flow parameter only changes if the coolant temperature changes, or if the geometry changes such as due to sand blockage. The percentage reduction in flow parameter $\%RFP$, due to sand blockage is given as:

$$\%RFP = \frac{FP_0 - FP}{FP_0} \tag{27}$$

Where FP_0 is the initial 'clean' flow parameter. This parameter allows experimental or numerical predictions of cooling hole blockage to be translated to full-scale engine performance predictions.

3.5.2 Cooling Effectiveness

The cooling effectiveness is a dimensionless parameter that gives an instantaneous evaluation of the success at which the film cooling is reducing the heat transfer from hot gas to blade. It is defined as:

$$\eta_C = \frac{T_g - T_b}{T_g - T_c} \tag{28}$$

Where T_g is the temperature of the hot-gas stream, T_b is the adiabatic blade wall temperature, and T_C is the coolant temperature. Rearranging Eq. 25 allows the blade temperature to be found, assuming the cooling effectiveness is known.

Igie et al.[40] state that the cooling effectiveness can be obtained empirically for various cooling techniques using a cooling mass flow function, defined as:

$$\dot{m}^* = \frac{\dot{m}_c}{\dot{m}_g} \frac{C_{p,c}}{C_{p,g}} \frac{1}{St_g} \frac{A_g}{N_c S_p L} \tag{29}$$

Where $\dot{m}_c$ is the coolant mass flow rate, $\dot{m}_g$ is the gas mass flow rate, $C_{p,c}$ is the coolant specific heat capacity, $C_{p,g}$ is the gas specific heat capacity, St_g is the gas Stanton number, A_g is the cross sectional area of the blade on which the bulk gas has an effect, N_c is the number of cooling channels per blade, S_b is the blade perimeter of the coolant channels of the blade, and L is the blade span.

3.5.3 Blade Lifetime

The consequence of ineffective cooling is an increase in blade operating temperature upon which the maximum allowable blade stress will strongly depend. Under tensile stress, the blade will undergo creep extension. For example, this maximum stress may therefore be specified as that stress at which the blade will not exceed a creep extension of 1% for 100,000 hours of operation at the temperature in question (Ref.[23]). Since all materials exhibit a loss of strength with temperature, blade cooling is essential if gas turbine inlet temperatures are to continue to rise for better fuel efficiency.

The Larson-Miller time temperature parameter is often used to evaluate the first rotor blade creep life due to turbine entry temperature increase, as described by Igie et al.[40]. It is based on the assumption that an increase in blade operating temperature will reduce the time taken to reach a particular creep state. The L-M parameter, P, is given as:

$$P = \frac{T_b}{1000}\left(\log_{10} t_f + C\right) \tag{30}$$

Where T_b is the blade operating temperature, t_f is the time to failure, and C is a material constant, given the value of 20 in this industrial application. (A value of C is sought for the blade material used in turboshaft engines).

Igie et al. investigated this for a two-spool engine, assuming uniform temperature throughout the blade chord and span and constant cooling effectiveness, among other constants. Clearly in the present case these assumptions cannot be made, but it is thought that this can be overcome by assuming a quasi-steady approach (reduction over time of the time to failure, t_f). The P value is known value that depends on the blade material.

3.6 Engine Model

The over-arching aim of the methodology proposed is to predict engine degradation due to sand ingestion, and relate this back to the physical and chemical properties of the contaminant. By using the equations presented, it should be possible to calculate to first order accuracy the effect of cooling hole blockage. This is done using the one-dimensional gas turbine path anaylsis tool Gas Simulation Program. The expected outputs are a transient loss of power, quantified by a power performance index, and a percentage reduction in surge margin.

4 Concluding Remarks

A methodology was proposed that draws on the existing literature on deposition in the hot end turbomachinery. More specifically, it employs existing empirical methods and analytical solutions to quantify the reduction in coolant mass flow and cooling effectiveness as a result of cooling hole blockage.

The rate of melting and sticking potential of ingested sand is dependent on its chemical properties, while the rate of ingestion of a given contaminant is dependent on its particle size distribution and subsequent Stokes number. Deposition at the turbine stage of a helicopter engine can occur within the cooling holes or on the surface of the nozzle guide vane or blade surface. The melting point is the key parameter to find, but is a function of the particle's mineralogy and is not simply a number. The softening of a material is an evolutionary process, governed by the proportion of mineral compounds in the sample. An important observation from the literature is that test sands, while being an appropriate surrogate for real sand in terms of size distribution, do not represent the chemical composition of the particles that evade capture by the EAPS system.

This methodology is being developed to better predict the degradation of engine performance.

5 References

[1] N. Bojdo and A. Filippone, "Comparative Study of Helicopter Engine Particle Separators," *Journal of Aircraft*, vol. 51, no. 3, pp. 1030–1042, 2014.

[2] Sgt Steve Blake RLC and UK Ministry of Defence, *RAF Merlin Helicopter Creates a "Brownout" Dust Cloud Landing in Afghanistan*. 2012.

[3] D. Barone, E. Loth, and P. Snyder, "Fluid Dynamics of an Inertial Particle Separator," 2014.

[4] P. H. Snyder, "Particle Separator for a Gas Turbine Engine," 6499285 B1, 31-Dec-2002.

[5] F. Saeed and A. Z. Al-Garni, "Analysis Method for Inertial Particle Separator," *Journal of Aircraft*, vol. 44, no. 4, pp. 1150–1158, 2007.

[6] G. O. Musgrove, M. D. Barringer, K. A. Thole, E. Grover, and J. Barker, "Computational design of a louver particle separator for gas turbine engines," *ASME Paper No. GT2009-60199, Proceedings of ASME Turbo Exp, Orlando, FL*, 2009.

[7] M. Taslim, A. Khanicheh, and S. Spring, "A Numerical Study of Sand Separation Applicable to Engine Inlet Particle Separator Systems," *Journal of the American Helicopter Society*, vol. 54, no. 4, pp. 42001–42001, 2009.

[8] J. L. Smialek, F. A. Archer, and R. G. Garlick, "Turbine airfoil degradation in the persian gulf war," *JOM*, vol. 46, no. 12, pp. 39–41, Dec. 1994.

[9] A. Hamed, W. Tabakoff, and R. Wenglarz, "Erosion and deposition in turbomachinery," *Journal of Propulsion and Power*, vol. 22, no. 2, pp. 350–360, 2006.

[10] W. Ai, N. Murray, T. H. Fletcher, S. Harding, S. Lewis, and J. P. Bons, "Deposition Near Film Cooling Holes on a High Pressure Turbine Vane," *Journal of Turbomachinery*, vol. 134, no. 4, p. 041013, 2012.

[11] C. R. Davison and T. A. Rutke, "Assessment and Characterization of Volcanic Ash Threat to Gas Turbine Engine Performance," *J. Eng. Gas Turbines Power*, vol. 136, no. 8, pp. 081201–081201, Mar. 2014.

[12] M. J. Scimone, D. Flesher, and S. Frey, "High Performance Barrier Filtration Systems," in *Proceedings of the 56th American Helicopter Society Annual Forum*, Virginia Beach, VA, 2000.

[13] J. P. Van Der Walt and A. Nurick, "Life prediction of helicopter engines fitted with dust filters," *J Aircraft*, vol. 32, no. 1, pp. 118–123, Jan. 1995.

[14] S. A. Lawson and K. A. Thole, "Effects of simulated particle deposition on film cooling," *Journal of Turbomachinery*, vol. 133, no. 2, p. 021009, 2011.

[15] M. Shinozaki, K. A. Roberts, B. van de Goor, and T. W. Clyne, "Deposition of Ingested Volcanic Ash on Surfaces in the Turbine of a Small Jet Engine," *Adv. Eng. Mater.*, vol. 15, no. 10, pp. 986–994, Oct. 2013.

[16] W. Song, K.-U. Hess, D. E. Damby, F. B. Wadsworth, Y. Lavallée, C. Cimarelli, and D. B. Dingwell, "Fusion characteristics of volcanic ash relevant to aviation hazards," *Geophys. Res. Lett.*, vol. 41, no. 7, p. 2013GL059182, Apr. 2014.

[17] G. B. Bessee and K. B. Kohl, "Characterization of CONUS and Saudi Arabian Fine-Grained Soil Samples," DTIC Document, 1993.

[18] S. Singh, D. Tafti, C. Reagle, J. Delimont, W. Ng, and S. Ekkad, "Sand transport in a two pass internal cooling duct with rib turbulators," *International Journal of Heat and Fluid Flow*, vol. 46, pp. 158–167, Apr. 2014.

[19] J. Kim, M. G. Dunn, A. J. Baran, D. P. Wade, and E. L. Tremba, "Deposition of Volcanic Materials in the Hot Sections of Two Gas Turbine Engines," *J. Eng. Gas Turbines Power*, vol. 115, no. 3, pp. 641–651, Jul. 1993.

[20] S. S. Sreedharan and D. K. Tafti, "Composition Dependent Model for the Prediction of Syngas Ash Deposition With Application to a Leading Edge Turbine Vane," in *ASME Turbo Expo 2010: Power for Land, Sea, and Air*, 2010, pp. 615–626.

[21] B. J. Barker, "Simulation of Coal Ash Deposition on Modern Turbine Nozzle Guide Vanes," The Ohio State University, 2010.

[22] W. S. Walsh, K. A. Thole, and C. Joe, "Effects of sand ingestion on the blockage of film-cooling holes," *GT2006-90067*, 2006.

[23] P. G. Hill and C. R. Peterson, *Mechanics and thermodynamics of propulsion*, vol. 1. Addison-Wesley, Reading, Massachusetts, 1992.

[24] A. Filippone and N. Bojdo, "Turboshaft engine air particle separation," *Progress in Aerospace Sciences*, vol. 46, no. 5–6, pp. 224–245, Jul. 2010.

[25] J. P. Van Der Walt and A. Nurick, "Erosion of Dust-Filtered Helicopter Turbine Engines Part II: Erosion Reduction," *J Aircraft*, vol. 32, no. 1, pp. 112–117, Jan. 1995.
[26] J. L. Smialek, F. A. Archer, and R. G. Garlick, "The chemistry of Saudi Arabian sand - A deposition problem on helicopter turbine airfoils," in *24th International SAMPE Technical Conference*, 1992, vol. 24, p. 63.
[27] C. Cowherd Jr, "Sandblaster 2 support of see-through technologies for particulate brownout," DTIC Document, 2007.
[28] J. Milluzzo and G. Leishman, "Assessment of Rotorcraft Brownout Severity in Terms of Rotor Design Parameters," *Journal of the American Helicopter Society*, vol. 55, no. 3, pp. 032009–1, 2010.
[29] B. Johnson, J. G. Leishman, and A. Sydney, "Investigation of Sediment Entrainment Using Dual-Phase, High-Speed Particle Image Velocimetry," *Journal of the American Helicopter Society*, vol. 55, no. 4, pp. 42003–42003, 2010.
[30] J.-C. Han, S. Dutta, and S. Ekkad, *Gas turbine heat transfer and cooling technology*. CRC Press, 2012.
[31] N. D. Cardwell, K. A. Thole, and S. W. Burd, "Investigation of Sand Blocking Within Impingement and Film-Cooling Holes," *J. Turbomach.*, vol. 132, no. 2, pp. 021020–021020, Jan. 2010.
[32] N. Sundaram and K. A. Thole, "Effects of Surface Deposition, Hole Blockage, and TBC Spallation on Vane Endwall Film-Cooling," in *ASME Turbo Expo 2006: Power for Land, Sea, and Air*, 2006, pp. 407–418.
[33] J. P. Bons, J. E. Wammack, J. Crosby, D. Fletcher, and T. H. Fletcher, "Evolution of Surface Deposits on a High-Pressure Turbine Blade—Part II: Convective Heat Transfer," *Journal of Turbomachinery*, vol. 130, no. 2, p. 021021, 2008.
[34] J. P. Bons, R. P. Taylor, S. T. McClain, and R. B. Rivir, "The many faces of turbine surface roughness," *Journal of Turbomachinery*, vol. 123, no. 4, pp. 739–748, 2001.
[35] C. Phillips, H. W. Kim, and R. E. Brown, "Helicopter brownout - Can it be modelled?," *Aeronautical Journal*, vol. 115, no. 1164, pp. 123–133, 2011.
[36] N. Bojdo, "Rotorcraft Engine Air Particle Separation," PhD Thesis, University of Manchester, 2012.
[37] A. Haider and O. Levenspiel, "Drag coefficient and terminal velocity of spherical and nonspherical particles," *Powder technology*, vol. 58, no. 1, pp. 63–70, 1989.
[38] K. Brun, M. Nored, and R. Kurz, "Particle Transport Analysis of Sand Ingestion in Gas Turbine Engines," *Journal of Engineering for Gas Turbines and Power*, vol. 134, p. 012402, 2012.
[39] S. Fotovati, H. V. Tafreshi, and B. Pourdeyhimi, "A macroscale model for simulating pressure drop and collection efficiency of pleated filters over time," *Separation and Purification Technology*, vol. 98, pp. 344–355, Sep. 2012.
[40] U. Igie and O. Minervino, "Impact of Inlet Filter Pressure Loss on Single and Two-Spool Gas Turbine Engines for Different Control Modes," *J. Eng. Gas Turbines Power*, vol. 136, no. 9, pp. 091201–091201, May 2014.

COPYRIGHT STATEMENT